Coupled Aeroelastic Vortex Lattice Modeling of Flexible Aircraft

Nhan Nguyen*
NASA Ames Research Center, Moffett Field, CA 94035
Khanh Trinh†
Stinger Ghaffarian Technologies Inc., NASA Ames Research Center, Moffett Field, CA 94035
Susan Frost‡
NASA Ames Research Center, Moffett Field, CA 94035
Kevin Reynolds§
NASA Ames Research Center, Moffett Field, CA 94035

This paper presents a recently developed computational tool for aeroelastic analysis of aircraft performance. The computational tool couples a vortex-lattice code, Vorview, with an aeroelastic model that computes wing structural deflections under a combined coupled bending-torsion motion. The aeroelastic model of the wing structure is based on a one-dimensional structural dynamic theory using steady state aerodynamics assumption. An automated aircraft geometry modeler is developed to generate a deformed aircraft geometry based on the structural deflection aeroelastic analysis. The computation is iterated until the solution converges within a specified error tolerance. This computational tool is capable to predict both steady state aerodynamics as well as aeroelastically induced unsteady aerodynamics. Simulations are conducted for a generic transport aircraft to demonstrate the capability of the computational tool.

I. Introduction

Light weight aircraft design has received a considerable attention in recent years as a means for improving cruise efficiency. Reducing aircraft weight results in lower lift requirement which directly translates into lower induced drag, hence reduced engine thrust requirement during cruise. The use of light-weight materials such as advanced composite materials has been adopted by airframe manufacturers in a number of current and future aircraft. Modern light-weight materials can provide less structural rigidity while maintaining sufficient load-carrying capacity. As structural flexibility increases, aeroelastic interactions with aerodynamic forces and moments become an increasingly important consideration in aircraft design. Understanding aeroelastic effects can improve the prediction of aircraft aerodynamic performance and provide an insight into how to design an aerodynamically efficient airframe that exhibits a high degree of flexibility. Moreover, there exist potential adverse interactions between airframe flexibility and dynamics of highly flexible aircraft that can compromise vehicle stability and control.

This paper describes a recent development of a computational capability that couples a static and dynamic aeroelastic model of aircraft wing structures with a vortex-lattice aerodynamic code for aerodynamic performance prediction. The aeroelastic model is based on one-dimensional structural dynamic theory that models a wing structure as a beam in a combined coupled bending-torsion motion. Aeroelastic analysis is performed based on the quasi-steady state aerodynamic assumption. The coupling between the aeroelastic model and the vortex-lattice code is made possible by a computational geometry model that updates the aircraft deformed geometry at each iteration.

*Research Scientist, Intelligent Systems Division, AIAA Associate Fellow
†Engineer, Stinger Ghaffarian Technologies Inc. (SGT Inc.)
‡Research Engineer, Intelligent Systems Division, AIAA Member
§Research Engineer, Intelligent Systems Division

II. Computational Tools

A. Vorview Vortex-Lattice Code

Vorview is a computational aerodynamic tool that is used for the development of the aeroelastic computational capability.[1] Vorview provides a rapid method for estimating aerodynamic force and moment coefficients as well as aerodynamic stability and control derivatives for a given aircraft configuration. It is based on the vortex-lattice lifting line aerodynamic theory. The vehicle configuration is constructed within Vorview by a series of panels that are formed by spanwise and chordwise locations of bound vortices. Vorview computes the vehicle aerodynamics in both the longitudinal and lateral directions independently. The longitudinal and lateral aerodynamics are then combined to produce overall aerodynamic characteristics of the vehicle at any arbitrary angle of attack and angle of sideslip. Due to the inviscid nature of any vortex-lattice method, the drag prediction by Vorview is most reliable for induced drag prediction. For viscous drag due to boundary layer separation or wave drag due to shock-induced boundary layer separation, the prediction may be less reliable. Vorview can provide a rapid estimation of aerodynamic derivatives including dynamic derivatives due to angular rates. Owing to the computationally efficient vortex-lattice method, aerodynamic derivatives can be estimated in Vorview fairly quickly. A flight dynamic model for a given vehicle configuration can be easily developed with Vorview that supplies the model with all necessary aerodynamic information for the vehicle.

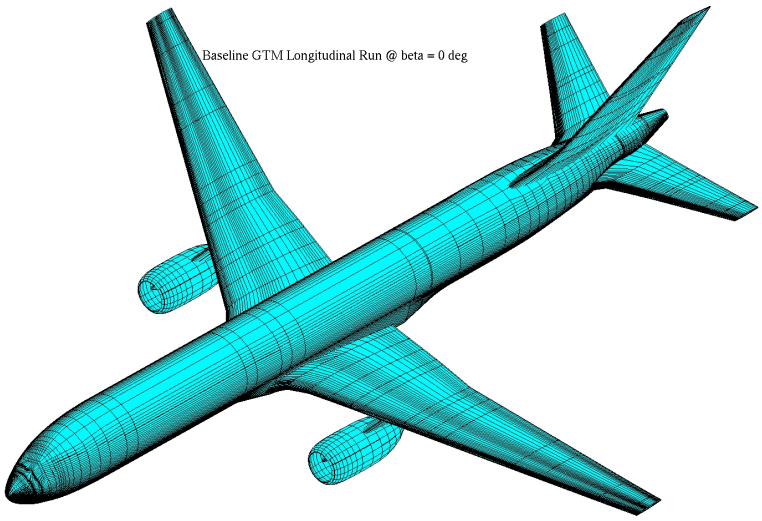

Figure 1 - Vorview Aircraft Model

Vorview has been validated by both wind tunnel data[2] as well as NASA Cart3D tool[3] which is a high-fidelity inviscid (Euler) CFD analysis code targeted at analyzing aircraft performance in conceptual and preliminary aerodynamic design. In general, both of these aerodynamic codes seem to have similar predictive capabilities when compressibility is not a factor. Figures 2 and 3 illustrate the comparison of lift and drag prediction of Vorview and Cart3D as compared to wind tunnel data for a Generic Transport Model (GTM) taken in NASA Langley's 14-By 22-Foot Wind Tunnel. In compressible simulations, Cart3D is expected to be substantially more accurate since the vortex panel method used by Vorview cannot account for compressibility effects (e.g. shock formation and wave-drag) within the flow.

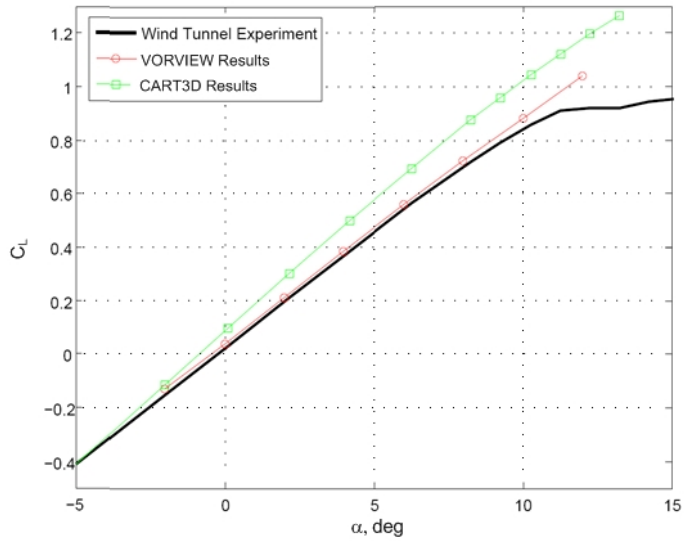

Figure 2 - C_L vs. α Comparison

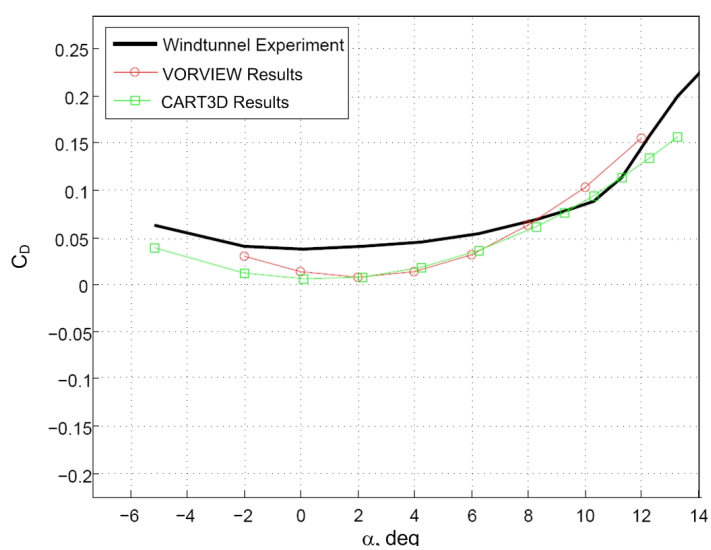

Figure 3 - C_D vs. α Comparison

B. Automated Vehicle Geometry Modeling Tool

To enable a coupled aeroelastic solution, the aircraft deformed geometry must be generated at each iteration. An automated vehicle geometry modeling tool has been developed in MATLAB to update the aircraft deformed geometry. The vehicle geometry modeler directly outputs a geometry input file that can be read by Vorview during a solution cycle. The vehicle geometry modeler has access to the outer mold line of the jig-shape (undeformed) aircraft geometry. The coordinate reference frame (x_V, y_V, z_V) defines the coordinate system used in the vehicle geometry model. Wing chordwise and flapwise bending deflection shapes and a twist distribution are superimposed on top of the wing geometry as shown in Figure 4. A deformed wing geometry is generated by a coordinate transformation as follows:

1. A coordinate rotation to account for twist is performed first by rotating a jig-shape wing section about its area center by a specified twist angle at a given y_V-coordinate. The transformed coordinates due to twist are computed as

$$x_V^{'} = \bar{x} + (x_V - \bar{x})\cos\Theta(y_V) - (z_V - \bar{z})\sin\Theta(y_V) \tag{1}$$

$$z_V^{'} = \bar{z} + (x_V - \bar{x}) \sin\Theta(y_V) + (z_V - \bar{z}) \cos\Theta(y_V) \tag{2}$$

where Θ is the twist angle, positive nose-down and negative nose-up.

2. A coordinate translation in the x_V-direction to account for chordwise bending is performed next by translating the previously transformed $x_V^{'}$-coordinate by a specified chordwise bending deflection at a given y_V-coordinate. The transformed coordinates due to chordwise bending are computed as

$$x_V^{''} = x_V^{'} + V(y_V) \tag{3}$$

$$z_V^{''} = z_V^{'} \tag{4}$$

where V is the chordwise bending deflection, positive swept back and negative swept forward.

3. Finally, a coordinate translation in the z_V-direction to account for flapwise bending is performed by translating the previously transformed $z_V^{''}$ by a specified flapwise bending deflection at a given y_V-coordinate. The transformed coordinates due to flapwise bending are computed as

$$x_V^{'''} = x_V^{''} \tag{5}$$

$$z_V^{'''} = z_V^{''} + W(y_V) \tag{6}$$

where W is the flapwise bending deflection, positive up and negative down.

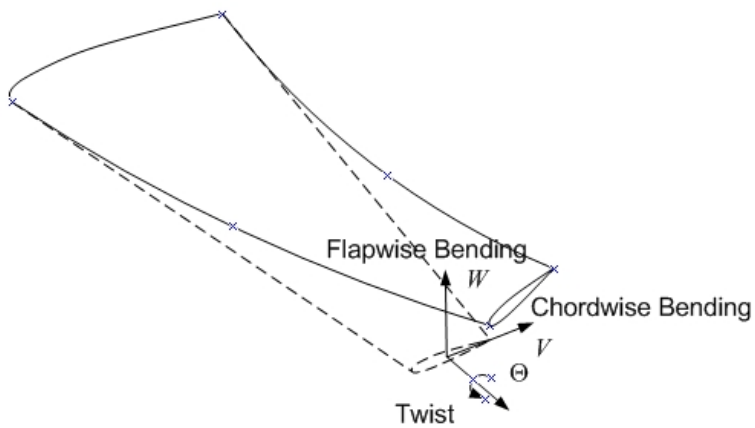

Figure 4 - Wing Bending Deflections and Twist

III. Aeroelastic Modeling

Aeroelasticity theory is used to develop a structural deflection model of an aircraft wing structure undergoing a combined coupled bending-torsion motion. The model uses the aerodynamic information generated from Vorview to compute the aeroelastic deflections of the wing structure in bending and torsion. The aeroelastic deflections are then used by the automated vehicle geometry modeler to update the aircraft geometry in Vorview with the deformed wing shape. The deformed aircraft model is then iterated between Vorview and the aeroelastic model until the static solution of the aeroelastic deflections converge.

A. Reference Frames

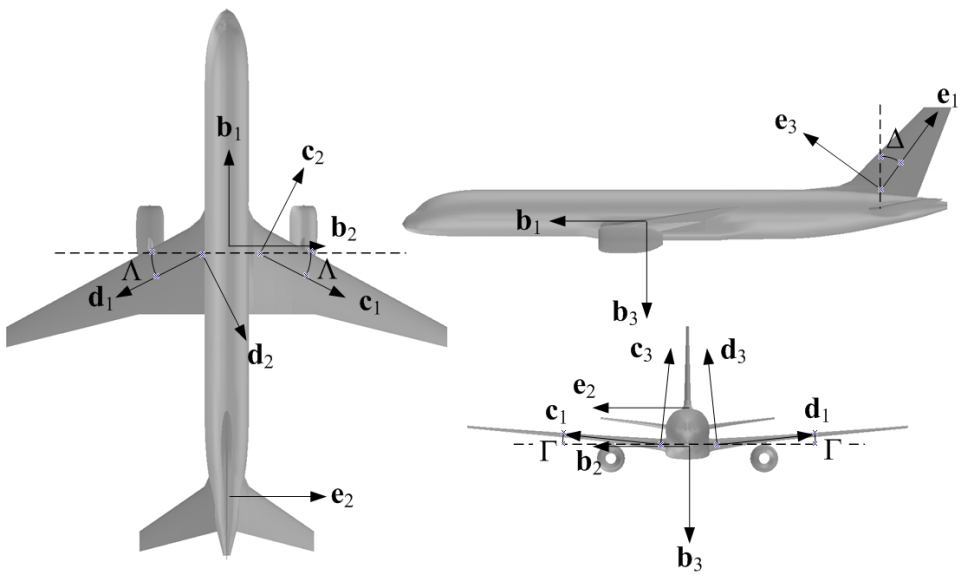

Figure 5 - Aircraft Reference Frames

Figure 5 illustrates three orthogonal views of a typical aircraft. Several reference frames are introduced to facilitate the rigid-body dynamic and structural dynamic analysis of the lifting surfaces. For example, the aircraft inertial reference frame A is defined by unit vectors $\mathbf{a}_1$, $\mathbf{a}_2$, and $\mathbf{a}_3$ fixed to the non-rotating earth. The aircraft body-fixed reference frame B is defined by unit vectors $\mathbf{b}_1$, $\mathbf{b}_2$, and $\mathbf{b}_3$. The reference frames A and B are related by three successive rotations: 1) the first rotation about $\mathbf{a}_3$ by the heading angle ψ that results in an intermediate reference frame A$'$ defined by unit vectors $\mathbf{a}_1'$, $\mathbf{a}_2'$, and $\mathbf{a}_3'$ (not shown), 2) the second rotation about $\mathbf{a}_2'$ by the pitch angle θ that results in an intermediate reference frame B$'$ defined by unit vectors $\mathbf{b}_1'$, $\mathbf{b}_2'$, and $\mathbf{b}_3'$ (not shown), and 3) the third rotation about $\mathbf{b}_1'$ by the bank angle ϕ that results in the reference frame B. This relationship can be expressed as

$$\begin{bmatrix} \mathbf{a}_1 \\ \mathbf{a}_2 \\ \mathbf{a}_3 \end{bmatrix} = \begin{bmatrix} \cos\psi & -\sin\psi & 0 \\ \sin\psi & \cos\psi & 0 \\ 0 & 0 & 1 \end{bmatrix} \begin{bmatrix} \cos\theta & 0 & \sin\theta \\ 0 & 1 & 0 \\ -\sin\theta & 0 & \cos\theta \end{bmatrix} \begin{bmatrix} 1 & 0 & 0 \\ 0 & \cos\phi & -\sin\phi \\ 0 & \sin\phi & \cos\phi \end{bmatrix} \begin{bmatrix} \mathbf{b}_1 \\ \mathbf{b}_2 \\ \mathbf{b}_3 \end{bmatrix}$$
$$= \begin{bmatrix} \cos\psi\cos\theta & -\sin\psi\cos\phi + \cos\psi\sin\theta\sin\phi & \sin\psi\sin\phi + \cos\psi\sin\theta\cos\phi \\ \sin\psi\cos\theta & \cos\psi\cos\phi + \sin\psi\sin\theta\sin\phi & -\cos\psi\sin\phi + \sin\psi\sin\theta\cos\phi \\ -\sin\theta & \cos\theta\sin\phi & \cos\theta\cos\phi \end{bmatrix} \begin{bmatrix} \mathbf{b}_1 \\ \mathbf{b}_2 \\ \mathbf{b}_3 \end{bmatrix} \tag{7}$$

The left wing elastic reference frame D is defined by unit vectors $\mathbf{d}_1$, $\mathbf{d}_2$, and $\mathbf{d}_3$. The reference frames B and D are related by three successive rotations: 1) the first rotation about $\mathbf{b}_3$ by the elastic axis sweep angle $\frac{3\pi}{2} - \Lambda$ that results in an intermediate reference frame B$''$ defined by unit vectors $\mathbf{b}_1''$, $\mathbf{b}_2''$, and $\mathbf{b}_3''$ (not shown), 2) the second rotation about negative $\mathbf{b}_2''$ by the elastic axis dihedral angle Γ that results in an intermediate reference frame D$'$ defined by unit vectors $\mathbf{d}_1'$, $\mathbf{d}_2'$, and $\mathbf{d}_3'$ (not shown), and 3) the third rotation about $\mathbf{d}_1'$ by an angle π that results in the reference frame D. This relationship can be expressed as

$$\begin{bmatrix} \mathbf{b}_1 \\ \mathbf{b}_2 \\ \mathbf{b}_3 \end{bmatrix} = \begin{bmatrix} -\sin\Lambda & \cos\Lambda & 0 \\ -\cos\Lambda & -\sin\Lambda & 0 \\ 0 & 0 & 1 \end{bmatrix} \begin{bmatrix} \cos\Gamma & 0 & -\sin\Gamma \\ 0 & 1 & 0 \\ \sin\Gamma & 0 & \cos\Gamma \end{bmatrix} \begin{bmatrix} 1 & 0 & 0 \\ 0 & -1 & 0 \\ 0 & 0 & -1 \end{bmatrix} \begin{bmatrix} \mathbf{d}_1 \\ \mathbf{d}_2 \\ \mathbf{d}_3 \end{bmatrix}$$
$$= \begin{bmatrix} -\sin\Lambda\cos\Gamma & -\cos\Lambda & -\sin\Lambda\sin\Gamma \\ -\cos\Lambda\cos\Gamma & \sin\Lambda & \cos\Lambda\sin\Gamma \\ \sin\Gamma & 0 & -\cos\Gamma \end{bmatrix} \begin{bmatrix} \mathbf{d}_1 \\ \mathbf{d}_2 \\ \mathbf{d}_3 \end{bmatrix} \tag{8}$$

Generally, the effect of the dihedral angle can be significant. A full analysis with the dihedral angle can be performed but can also result in a very complex analytical formulation. Thus, to simplify the analysis, the dihedral

effect is assumed to be negligible in this study. The right wing reference frame C can be established in a similar manner. In the analysis, the aeroelastic effects on the fuselage, horizontal stabilizers, and vertical stabilizer are not considered, but the analytical method can be formulated for analyzing these lifting surfaces if necessary. In general, a whole aircraft analysis approach should be conducted to provide a comprehensive assessment of the effect of structural flexibility on aircraft performance and stability. However, the scope of this study pertains to only the wing structures.

B. Elastic Analysis

In the subsequent analysis, the combined motion of the left wing is considered. The motion of the right wing is a mirror image of that of the left wing for symmetric flight. The wing has a varying pre-twist angle $\gamma(x)$ commonly designed in many aircraft. Typically, the wing pre-twist angle varies from being nose-up at the wing root to nose-down at the wing tip. The nose-down pre-twist at the wing tip is designed to delay stall onsets. This is called a wash-out twist distribution. Under aerodynamic forces and moments, the aeroelastic deflections of a wing introduce stresses and strains into the wing structure. The internal structure of a wing typically comprises a complex arrangement of load carrying spars and wing boxes. Nonetheless, the elastic behavior of a wing can be captured by the use of equivalent stiffness properties. These properties can be derived from structural certification testing that yields information about wing deflections as a function of loading. For high aspect ratio wings, an equivalent beam approach can be used to analyze aeroelastic deflections with good accuracy. The equivalent beam approach is a typical formulation in many aeroelasticity studies.[4] It is assumed that the effect of wing curvature is ignored and the straight beam theory is used to model the wing deflection.

Consider an airfoil section on the left wing as shown in Figure 6 undergoing bending and torsional deflections.

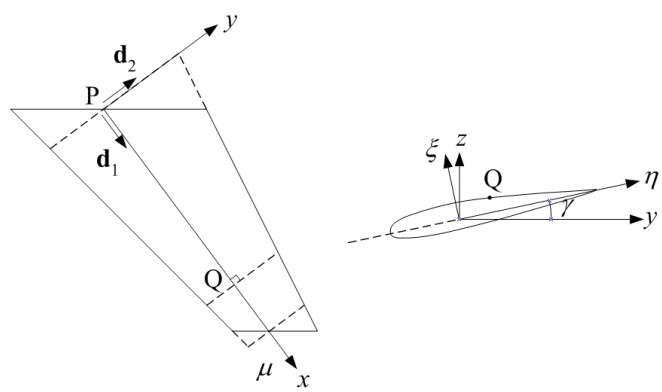

Figure 6 - Left Wing Reference Frame

Let (x, y, z) be the coordinates of a point Q on the airfoil. Then the undeformed local airfoil coordinates of point Q are

$$\begin{bmatrix} y \\ z \end{bmatrix} = \begin{bmatrix} \cos\gamma & -\sin\gamma \\ \sin\gamma & \cos\gamma \end{bmatrix} \begin{bmatrix} \eta \\ \xi \end{bmatrix} \tag{9}$$

where η and ξ are local airfoil coordinates, and γ is the wing section pre-twist angle, positive nose-down.[5]

Then differentiating with respect to x gives

$$\begin{bmatrix} y_x \\ z_x \end{bmatrix} = \gamma' \begin{bmatrix} -\sin\gamma & -\cos\gamma \\ \cos\gamma & -\sin\gamma \end{bmatrix} \begin{bmatrix} \eta \\ \xi \end{bmatrix} = \begin{bmatrix} -z\gamma' \\ y\gamma' \end{bmatrix} \tag{10}$$

The axial or extensional deflection of a wing is generally very small and therefore can usually be neglected. Let Θ be a torsional twist angle about the x-axis, positive nose-down, and let W and V be flapwise and chordwise bending deflections of point Q, respectively.. Then, the rotation angle due to the elastic deformation can be expressed as

$$\phi(x,t) = \Theta\mathbf{d}_1 - W_x\mathbf{d}_2 + V_x\mathbf{d}_3 \tag{11}$$

where the subscripts x and t denote the partial derivatives of Θ, W, and V.

Let (x_1, y_1, z_1) be the coordinates of point Q on the airfoil in the reference frame D. Then the coordinates (x_1, y_1, z_1) are computed using the small angle approximation as

$$\begin{bmatrix} x_1(x,t) \\ y_1(x,t) \\ z_1(x,t) \end{bmatrix} = \begin{bmatrix} x \\ y+V \\ z+W \end{bmatrix} + \begin{bmatrix} \phi \times (y\mathbf{d}_2 + z\mathbf{d}_3).\mathbf{d}_1 \\ \phi \times (y\mathbf{d}_2 + z\mathbf{d}_3).\mathbf{d}_2 \\ \phi \times (y\mathbf{d}_2 + z\mathbf{d}_3).\mathbf{d}_3 \end{bmatrix} = \begin{bmatrix} x - yV_x - zW_x \\ y + V - z\Theta \\ z + W + y\Theta \end{bmatrix} \tag{12}$$

Differentiating x_1, y_1, and z_1 with respect to x yields

$$\begin{bmatrix} x_{1,x} \\ y_{1,x} \\ z_{1,x} \end{bmatrix} = \begin{bmatrix} 1 - yV_{xx} + z\gamma' V_x - zW_{xx} - y\gamma' W_x \\ -z\gamma' + V_x - z\Theta_x - y\gamma'\Theta \\ y\gamma' + W_x + y\Theta_x - z\gamma'\Theta \end{bmatrix} \tag{13}$$

Neglecting the transverse shear effect, the longitudinal strain is computed as[6]

$$\varepsilon = \frac{ds_1 - ds}{ds} = \frac{s_{1,x}}{s_x} - 1 \tag{14}$$

where

$$s_x = \sqrt{1 + y_x^2 + z_x^2} = \sqrt{1 + (y^2 + z^2)(\gamma')^2} \tag{15}$$

$$s_{1,x} = \sqrt{x_{1,x}^2 + y_{1,x}^2 + z_{1,x}^2} = \sqrt{1 + (y^2 + z^2)(\gamma')^2 - 2yV_{xx} - 2zW_{xx} + 2(y^2 + z^2)\gamma'\Theta_x} \tag{16}$$

For a small wing twist angle γ, the longitudinal strain is obtained as

$$\varepsilon = -yV_{xx} - zW_{xx} + \left(y^2 + z^2\right)\gamma'\Theta_x \tag{17}$$

The moments acting on the wing are then obtained as

$$\begin{bmatrix} M_x \\ M_y \\ M_z \end{bmatrix} = \begin{bmatrix} GJ\Theta_x \\ 0 \\ 0 \end{bmatrix} + \iint E\varepsilon \begin{bmatrix} \left(y^2 + z^2\right)\left(\gamma' + \Theta_x\right) \\ -z \\ -y \end{bmatrix} dydz \tag{18}$$

$$= \begin{bmatrix} GJ + EB_1\left(\gamma'\right)^2 & -EB_2\gamma' & -EB_3\gamma' \\ -EB_2\gamma' & EI_{yy} & -EI_{yz} \\ -EB_3\gamma' & -EI_{yz} & EI_{zz} \end{bmatrix} \begin{bmatrix} \Theta_x \\ W_{xx} \\ V_{xx} \end{bmatrix} \tag{19}$$

where E is the Young's modulus; G is the shear modulus; γ' is the derivative of the wing pre-twist angle; I_{yy}, I_{yz}, and I_{zz} are the section area moments of inertia about the flapwise axis; J is the torsional constant; and B_1, B_2, and B_3 are the bending-torsion coupling constants which are defined as

$$\begin{bmatrix} B_1 \\ B_2 \\ B_3 \end{bmatrix} = \iint \left(y^2 + z^2\right) \begin{bmatrix} y^2 + z^2 \\ z \\ y \end{bmatrix} dydz \tag{20}$$

The strain analysis shows that, for a pre-twisted wing, the bending deflections are coupled to the torsional deflection via the slope of the wing pre-twist angle. This coupling can be significant if the wash-out slope γ' is dominant as in highly twisted wings such as turbomachinery blades. For an aircraft wing structure, a simplification can be made by neglecting the chordwise bending deflection. Thus, the resulting moments are now given as

$$\begin{bmatrix} M_x \\ M_y \end{bmatrix} = \begin{bmatrix} GJ + EB_1\left(\gamma'\right)^2 & -EB_2\gamma' \\ -EB_2\gamma' & EI_{yy} \end{bmatrix} \begin{bmatrix} \Theta_x \\ W_{xx} \end{bmatrix} \tag{21}$$

C. Aeroelastic Angle of Attack

The relative velocity of the air approaching a wing section includes the contribution from the wing elastic deflection that results in changes in the local angle of attack. Since aerodynamic forces and moments are dependent on the local angle of attack, the wing aeroelastic deflections will generate additional elastic forces and moments. The local angle of attack depends on the relative approaching air velocity as well as the rotation angle ϕ from Eq. (11). The relative air velocity in turn also depends on the deflection-induced velocity. The local velocity components at point Q in the reference frame D are given by[5]

$$\begin{bmatrix} v_x \\ v_y \\ v_z \end{bmatrix} = \begin{bmatrix} -u\sin\Lambda + x_{1,t} \\ -u\cos\Lambda + y_{1,t} \\ -w - qx_a + z_{1,t} \end{bmatrix} = \begin{bmatrix} -u\sin\Lambda - zW_{xt} \\ -u\cos\Lambda - z\Theta_t \\ -w - qx_a + W_t + y\Theta_t \end{bmatrix} \tag{22}$$

where $u \approx V_\infty$, $w \approx V_\infty \alpha$, q is the aircraft pitch rate, x_a is the position of point Q with respect to the aircraft C.G. (positive aft of C.G.) measured in the aircraft reference frame B, and y and z are coordinates of point Q in the reference frame D.

In order to compute the aeroelastic forces and moments, the velocity must be transformed from the reference frame D to the airfoil local coordinate reference frame defined by (μ, η, ξ) (see Figure 9). Then the transformation can be performed using two successive rotation matrix multiplication operations as

$$\begin{aligned} \begin{bmatrix} v_\mu \\ v_\eta \\ v_\xi \end{bmatrix} &= \begin{bmatrix} 1 & 0 & 0 \\ 0 & \cos(\Theta+\gamma) & \sin(\Theta+\gamma) \\ 0 & -\sin(\Theta+\gamma) & \cos(\Theta+\gamma) \end{bmatrix} \begin{bmatrix} \cos W_x & 0 & \sin W_x \\ 0 & 1 & 0 \\ -\sin W_x & 0 & \cos W_x \end{bmatrix} \begin{bmatrix} v_x \\ v_y \\ v_z \end{bmatrix} \\ &= \begin{bmatrix} v_x \cos W_x + v_z \sin W_x \\ -v_x \sin W_x \sin(\Theta+\gamma) + v_y \cos(\Theta+\gamma) + v_z \cos W_x \sin(\Theta+\gamma) \\ -v_x \sin W_x \cos(\Theta+\gamma) - v_y \sin(\Theta+\gamma) + v_z \cos W_x \cos(\Theta+\gamma) \end{bmatrix} \end{aligned} \tag{23}$$

For small deflections, the local velocity components can be simplified as

$$\begin{bmatrix} v_\mu \\ v_\eta \\ v_\xi \end{bmatrix} = \begin{bmatrix} v_x + v_z W_x \\ v_y + v_z(\Theta+\gamma) \\ v_z - v_x W_x - v_y(\Theta+\gamma) \end{bmatrix} \tag{24}$$

Referring to Figure 7, the local aeroelastic angle of attack on the airfoil section due to the velocity components v_η and v_ξ in the reference frame D is computed as

$$\alpha_c = \frac{v_\xi}{v_\eta} = \frac{\bar{v}_\xi + \Delta v_\xi}{\bar{v}_\eta + \Delta v_\eta} \tag{25}$$

where

$$\bar{v}_\xi = -w - qx_a \tag{26}$$

$$\bar{v}_\eta = -u\cos\Lambda \tag{27}$$

$$\Delta v_\xi = W_t + y\Theta_t - v_x W_x - v_y(\Theta+\gamma) \tag{28}$$

$$\Delta v_\eta = -z\Theta_t + v_z(\Theta+\gamma) \tag{29}$$

Then the local aeroelastic angle of attack can be evaluated as

$$\alpha_c = \frac{v_\xi}{\bar{v}_\eta} - \frac{\bar{v}_\xi \Delta v_\eta}{\bar{v}_\eta^2} = \frac{-w - qx_a + W_t + y\Theta_t - v_x W_x - v_y(\Theta+\gamma)}{-u\cos\Lambda} - \frac{(-w-qx_a)\left[-z\Theta_t + v_z(\Theta+\gamma)\right]}{u^2\cos^2\Lambda} \tag{30}$$

Ignoring the nonlinear terms, the expression for the local aeroelastic angle of attack is obtained as[5]

$$\alpha_c(x,y,z) = \frac{\alpha}{\cos\Lambda} + \frac{qx_a}{V_\infty\cos\Lambda} - \gamma(x) - W_x\tan\Lambda - \Theta - \frac{W_t + y\Theta_t}{V_\infty\cos\Lambda} - \frac{(w+qx_a)\left[z\Theta_t + (w+qx_a)(\Theta+\gamma)\right]}{u^2\cos^2\Lambda} \tag{31}$$

The terms W_t and Θ_t contribute to aerodynamic damping forces which can be significant for aeroelastic stability.

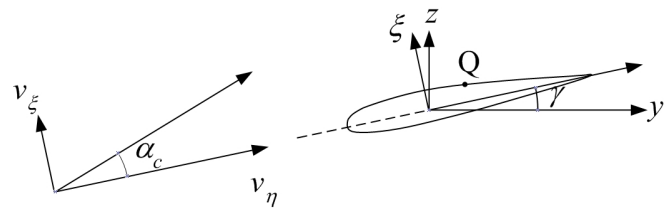

Figure 7 - Aeroelastic Angle of Attack

For aeroelastic analysis, the steady state aerodynamic method assumes that the steady state lift circulation occurs at the aerodynamic center of the oscillating airfoil, which may be taken to be the quarter-point. On the other hand, the unsteady aerodynamic method assumes that the unsteady circulation acts at the 3/4-chord point.[5] Both the Theodorsen's method for simple harmonic airfoil motion[7] and Peters' finite-state method can be used to analyze unsteady aerodynamics.[4] Based on the steady state aerodynamic assumption, the local angle of attack of an airfoil section at the elastic axis is evaluated at $y = -e$ and $z = 0$. Neglecting the last term, the expression for α_c is

$$\alpha_c(x) = \frac{\alpha}{\cos\Lambda} + \frac{q x_{ac}}{V_\infty \cos\Lambda} - \gamma(x) - W_x \tan\Lambda - \Theta - \frac{W_t - e\Theta_t}{V_\infty \cos\Lambda} \tag{32}$$

where x_{ac} is the distance from aircraft C.G. to the quarter-chord point measured in aircraft reference frame B (positive aft of C.G.) e is the distance between the quarter-chord point and the elastic axis.

For unsteady aerodynamics, the local angle of attack is evaluated at $y = b\left(\frac{1}{2} - a\right)$

$$\alpha_c(x) = \frac{\alpha}{\cos\Lambda} + \frac{q x_{ac}}{V_\infty \cos\Lambda} - \gamma(x) - W_x \tan\Lambda - \Theta - \frac{W_t + b\left(\frac{1}{2} - a\right)\Theta_t}{V_\infty \cos\Lambda} \tag{33}$$

where b is the half-chord length and $-1 \le a \le 1$ is a parameter such that the elastic axis is located at a distance $-ab$ from the mid-chord and $a < 0$ when the elastic axis is forward of the mid-chord.

In the present computational approach, the steady state aerodynamic method is used in the aeroelastic analysis. It is also noted that the three-dimensional lifting line effect that gives rise to the induced angle of attack is neglected in the analysis.

D. Wing Aeroelasticity

The wing deformation is comprised of two components: bending deflection $W(x)$ and torsional deflection $\Theta(x)$, where x is the wing local elastic axis. Furthermore, these deflections include both the static and dynamic contributions. Thus

$$\Theta(x,t) = \bar{\Theta}(x) + \Delta\Theta(x,t) \tag{34}$$

$$W(x,t) = \bar{W}(x) + \Delta W(x,t) \tag{35}$$

where $\bar{W}(x)$ and $\bar{\Theta}(x)$ are the static bending and torsional deflections, and $\Delta W(x,t)$ and $\Delta\Theta(x,t)$ are the dynamic bending and torsional deflections.

The equilibrium conditions for bending and torsion are expressed as

$$\frac{\partial M_x}{\partial x} = -m_x \tag{36}$$

$$\frac{\partial^2 M_y}{\partial x^2} = f_z - \frac{\partial m_y}{\partial x} \tag{37}$$

where m_x is the pitching moment per unit span about the elastic axis, f_z is the lift force per unit span, and m_y is the bending moment per unit span about the flapwise axis of the wing which is assumed to be zero.

The local pitching moment and lift coefficients are given by

$$c_m(x) = c_{m_{ac}} + \frac{e}{c}\left[c_{L_0} + c_{L_\alpha}\alpha_c(x)\right] + \sum_{k=1}^{m}\left(c_{m_{\delta_k}} + \frac{e}{c}c_{L_{\delta_k}}\right)\delta_k \tag{38}$$

$$c_L(x) = c_{L_0} + c_{L_\alpha}\alpha_c(x) + c_{L_\delta}\delta \tag{39}$$

where $c_{m_{ac}}$ is the section pitching moment coefficient about the section at the quarter-chord point at trim which is usually small and thus may be assumed to be zero, c_{L_0} is the section lift coefficient at zero angle of attack, c_{L_α} is the section lift vs. angle of attack curve slope, c is the section chord, δ_k is the surface deflection of the k-th flap, and $c_{L_{\delta_k}}$ and $c_{m_{\delta_k}}$ are the section lift and pitching moment control derivative at the quarter-chord point due to the k-th flap.

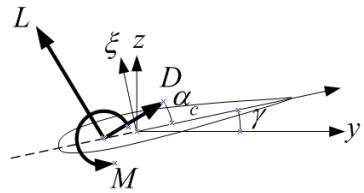

Figure 8 - Airfoil Forces and Moment

Using the sign convention as shown in Figure 8, the pitching moment per unit span can now be expressed as

$$m_x = -\left[c_{L_0} + c_{L_\alpha}\left(\frac{\alpha}{\cos\Lambda} + \frac{qx_{ac}}{V_\infty\cos\Lambda} - \gamma - W_x\tan\Lambda - \Theta - \frac{W_t - e\Theta_t}{V_\infty\cos\Lambda}\right) + \sum_{k=1}^{m}\left(\frac{c}{e}c_{m_{\delta_k}} + c_{L_{\delta_k}}\right)\delta_k\right] eq_\infty\cos^2\Lambda c + \rho gAe_{cg} - \rho I_{xx}\Theta_{tt} + \rho Ae_{cg}W_{tt} \quad (40)$$

where q_∞ is the dynamic pressure, ρ is the wing material density including fuel density, A is the cross sectional area of a wing section, e_{cg} is the eccentricity between the center of mass and the elastic axis (positive corresponding to the center of mass located forward of the elastic axis), I_{xx} is the section polar area moment of inertia, and the term $\cos^2\Lambda$ accounts for the wing sweep angle Λ as measured from the elastic axis.

The lift force per unit span is given by

$$f_z = \left[c_{L_0} + c_{L_\alpha}\left(\frac{\alpha}{\cos\Lambda} + \frac{qx_{ac}}{V_\infty\cos\Lambda} - \gamma - W_x\tan\Lambda - \Theta - \frac{W_t - e\Theta_t}{V_\infty\cos\Lambda}\right) + \sum_{k=1}^{m} c_{L_{\delta_k}}\delta_k\right] q_\infty\cos^2\Lambda c - \rho gA - \rho AW_{tt} + \rho Ae_{cg}\Theta_{tt} \quad (41)$$

where A is the cross sectional area of a wing section.

The bending and torsion aeroelastic equations then become

$$\frac{\partial}{\partial x}\left\{\left[GJ + EB_1\left(\gamma'\right)^2\right]\Theta_x - EB_2\gamma' W_{xx}\right\} = \left[c_{L_0} + c_{L_\alpha}\left(\frac{\alpha}{\cos\Lambda} + \frac{qx_{ac}}{V_\infty\cos\Lambda} - \gamma - W_x\tan\Lambda - \Theta - \frac{W_t - e\Theta_t}{V_\infty\cos\Lambda}\right) + \sum_{k=1}^{m}\left(\frac{c}{e}c_{m_{\delta_k}} + c_{L_{\delta_k}}\right)\delta_k\right] eq_\infty\cos^2\Lambda c - \rho gAe_{cg} + \rho I_{xx}\Theta_{tt} - \rho Ae_{cg}W_{tt} \quad (42)$$

$$\frac{\partial^2}{\partial x^2}\left(-EB_2\gamma'\Theta_x + EI_{yy}W_{xx}\right) = \left[c_{L_0} + c_{L_\alpha}\left(\frac{\alpha}{\cos\Lambda} + \frac{qx_{ac}}{V_\infty\cos\Lambda} - \gamma - W_x\tan\Lambda - \Theta - \frac{W_t - e\Theta_t}{V_\infty\cos\Lambda}\right) + \sum_{k=1}^{m} c_{L_{\delta_k}}\delta_k\right] q_\infty\cos^2\Lambda c - \rho gA - \rho AW_{tt} + \rho Ae_{cg}\Theta_{tt} \quad (43)$$

subject to fixed-end symmetric-mode boundary conditions $\Theta(0,t) = \Theta_x(L,t) = 0$ and $W(0,t) = W_x(0,t) = EIW_{xx}(L,t) = \frac{d}{dx}(EIW_{xx}(L,t)) = 0$, whereupon the x-coordinate of the wing elastic axis is translated such that the wing root section is at $x = 0$ and wing tip section is at $x = L$.

These equations describe the wing bending and torsional deflections due to aerodynamic forces and moments. Using the Galerkin's method,[8] the static and dynamic bending and torsional deflections can be approximated as

$$\bar{\Theta}(x) = \bar{\theta}\Psi_1(x) \quad (44)$$

$$\bar{W}(x) = \bar{w}\Phi_1(x) \tag{45}$$

$$\Delta\Theta(x,t) = \sum_{j=0}^{n} \theta_j(t)\Psi_j(x) \tag{46}$$

$$\Delta W(x,t) = \sum_{j=1}^{n} w_j(t)\Phi_j(x) \tag{47}$$

where $\bar{w}$ and $\bar{\theta}$ are the generalized coordinates for static bending and torsion, $\theta_j(t)$ and $w_j(t)$ are the generalized coordinates, and $\Psi_j(x)$ and $\Phi_j(x)$ are the assumed normalized eigenfunctions of the j-th bending and torsion aeroelastic modes, respectively, $j = 1,2,\ldots,n$.

The normalized eigenfunctions are given by

$$\Psi_j(x) = \sqrt{2}\sin\frac{(2j-1)\pi x}{2L} \tag{48}$$

$$\Phi_j(x) = \cosh(\beta_j x) - \cos(\beta_j x) - \frac{\cosh(\beta_j L)+\cos(\beta_j L)}{\sinh(\beta_j L)+\sin(\beta_j L)}\left[\sinh(\beta_j x) - \sin(\beta_j x)\right] \tag{49}$$

where $\beta_j L = 1.87510, 4.69409, \ldots$ is the eigenvalue of the j-th bending mode of a uniform cantilever beam, and the eigenfunctions $\Psi_j(x)$ and $\Phi_j(x)$ satisfy the orthogonal condition

$$\int_0^L \Psi_i(x)\Psi_j(x)\,dx = \int_0^L \Phi_i(x)\Phi_j(x)\,dx = \begin{cases} L & i = j \\ 0 & i \neq j \end{cases} \tag{50}$$

1. Static Analysis

The unsteady motion of the wing results in a time-varying angle of attack as

$$\alpha(t) = \bar{\alpha} + \Delta\alpha(t) \tag{51}$$

where $\bar{\alpha}$ is a trim angle of attack and $\Delta\alpha$ is a time-varying incremental angle of attack.

The flap deflection is generally time-varying resulting from flight control actions, and therefore can be decomposed into a steady state component and time-varying component as follows:

$$\delta_k(t) = \bar{\delta}_k + \Delta\delta_k(t) \tag{52}$$

where $\bar{\delta}_k$ is the trim flap deflection and $\Delta\delta_k$ is a time-varying incremental flap deflection.

For steady state motion, both the time-varying incremental angle of attack and the pitch rate are zero. Therefore, the static bending and torsion aeroelastic equations are expressed as

$$\frac{d}{dx}\left\{\left[GJ + EB_1\left(\gamma'\right)^2\right]\bar{\Theta}' - EB_2\gamma'\bar{W}''\right\} = \left[c_{L_0} + c_{L_\alpha}\left(\frac{\bar{\alpha}}{\cos\Lambda} - \gamma - \bar{W}'\tan\Lambda - \bar{\Theta}\right) + \sum_{k=1}^{m}\left(\frac{c}{e}c_{m_{\delta_k}} + c_{L_{\delta_k}}\right)\bar{\delta}_k\right] eq_\infty\cos^2\Lambda c - \rho g A e_{cg} \tag{53}$$

$$\frac{d^2}{dx^2}\left(-EB_2\gamma'\Theta_x + EI_{yy}W_{xx}\right) = \left[c_{L_0} + c_{L_\alpha}\left(\frac{\bar{\alpha}}{\cos\Lambda} - \gamma - \bar{W}'\tan\Lambda - \bar{\Theta}\right) + \sum_{k=1}^{m} c_{L_{\delta_k}}\bar{\delta}_k\right] q_\infty\cos^2\Lambda c - \rho g A \tag{54}$$

The weak-form integral expressions of the aeroelastic equations are obtained by multiplying the bending and torsion aeroelastic equations by $\Phi_1(x)$ and $\Psi_1(x)$, respectively, and then integrating over the wing span. This yields

$$\int_0^L \Psi_1\frac{d}{dx}\left\{\left[GJ + EB_1\left(\gamma'\right)^2\right]\bar{\theta}\Psi_1' - EB_2\gamma'\bar{w}\Phi_1''\right\}dx = \int_0^L \Psi_1\left[c_{L_0} + c_{L_\alpha}\left(\frac{\bar{\alpha}}{\cos\Lambda} - \gamma - \bar{w}\Phi_1'\tan\Lambda - \bar{\theta}\Psi_1\right) + \sum_{k=1}^{m}\left(\frac{c}{e}c_{m_{\delta_k}} + c_{L_{\delta_k}}\right)\bar{\delta}_k\right] eq_\infty\cos^2\Lambda c\,dx - \int_0^L \Psi_1\rho g A e_{cg}\,dx \tag{55}$$

$$\int_0^L \Phi_1 \frac{d^2}{dx^2}\left(-EB_2\gamma'\bar{\theta}\Psi_1' + EI_{yy}\bar{w}\Phi_1''\right)dx =$$
$$\int_0^L \Phi_1\left[c_{L_0} + c_{L_\alpha}\left(\frac{\bar{\alpha}}{\cos\Lambda} - \gamma - \bar{w}\Phi_1'\tan\Lambda - \bar{\theta}\Psi_1\right) + \sum_{k=1}^{m} c_{L_{\delta_k}}\bar{\delta}_k\right] q_\infty \cos^2\Lambda c dx - \int_0^L \Phi_1 \rho g A dx \quad (56)$$

The expressions of the left hand sides can be integrated by parts as

$$\int_0^L \Psi_1 \frac{d}{dx}\left\{\left[GJ + EB_1\left(\gamma'\right)^2\right]\bar{\theta}\Psi_1' - EB_2\gamma'\bar{w}\Phi_1''\right\}dx = \Psi_1\left\{\left[GJ + EB_1\left(\gamma'\right)^2\right]\bar{\theta}\Psi_1' - EB_2\gamma'\bar{w}\Phi_1''\right\}\Big|_0^L$$
$$- \int_0^L \Psi_1'\left\{\left[GJ + EB_1\left(\gamma'\right)^2\right]\bar{\theta}\Psi_1' - EB_2\gamma'\bar{w}\Phi_1''\right\}dx \quad (57)$$

$$\int_0^L \Phi_1 \frac{d^2}{dx^2}\left(-EB_2\gamma'\bar{\theta}\Psi_1' + EI_{yy}\bar{w}\Phi_1''\right)dx = \Phi_1\frac{d}{dx}\left(-EB_2\gamma'\bar{\theta}\Psi_1' + EI_{yy}\bar{w}\Phi_1''\right)\Big|_0^L$$
$$- \Phi_1'\left(-EB_2\gamma'\bar{\theta}\Psi_1' + EI_{yy}\bar{w}\Phi_1''\right)\Big|_0^L + \int_0^L \Phi_1''\left(-EB_2\gamma'\bar{\theta}\Psi_1' + EI_{yy}\bar{w}\Phi_1''\right)dx \quad (58)$$

Then, by enforcing the zero boundary conditions at the two end points, the weak-form static aeroelastic equations are obtained as

$$\int_0^L \Psi_1'\left\{\left[GJ + EB_1\left(\gamma'\right)^2\right]\bar{\theta}\Psi_1' - EB_2\gamma'\bar{w}\Phi_1''\right\}dx$$
$$+ \sum_{j=1}^{n}\int_0^L \Psi_1\left[c_{L_0} + c_{L_\alpha}\left(\frac{\bar{\alpha}}{\cos\Lambda} - \gamma - \bar{w}\Phi_1'\tan\Lambda - \bar{\theta}\Psi_1\right) + \sum_{k=1}^{m}\left(\frac{c}{e}c_{m_{\delta_k}} + c_{L_{\delta_k}}\right)\bar{\delta}_k\right] e q_\infty \cos^2\Lambda c dx - \int_0^L \Psi_1 \rho g A e_{cg} dx \quad (59)$$

$$\sum_{j=1}^{n}\int_0^L \Phi_1''\left(-EB_2\gamma'\bar{\theta}\Psi_1' + EI_{yy}\bar{w}\Phi_1''\right)dx$$
$$- \sum_{j=1}^{n}\int_0^L \Phi_1\left[c_{L_0} + c_{L_\alpha}\left(\frac{\bar{\alpha}}{\cos\Lambda} - \gamma - \bar{w}\Phi_1'\tan\Lambda - \bar{\theta}\Psi_1\right) + \sum_{k=1}^{m} c_{L_{\delta_k}}\bar{\delta}_k\right] q_\infty \cos^2\Lambda c dx + \int_0^L \Phi_1 \rho g A dx \quad (60)$$

These equations are expressed in a matrix form as

$$\begin{bmatrix} \bar{k}_{\theta\theta} & \bar{k}_{\theta w} \\ \bar{k}_{w\theta} & \bar{k}_{ww} \end{bmatrix}\begin{bmatrix} \bar{\theta} \\ \bar{w} \end{bmatrix} + \begin{bmatrix} \bar{h}_{\theta\alpha} \\ \bar{h}_{w\alpha} \end{bmatrix}\bar{\alpha} = \begin{bmatrix} \bar{f}_\theta \\ \bar{f}_w \end{bmatrix} + \sum_{k=1}^{m}\begin{bmatrix} \bar{g}_{\theta,k} \\ \bar{g}_{w,k} \end{bmatrix}\bar{\delta}_k \quad (61)$$

where

$$\bar{k}_{\theta\theta} = \int_0^L \left[GJ + EB_1\left(\gamma'\right)^2\right]\left(\Psi_1'\right)^2 dx - q_\infty \int_0^L c_{L_\alpha} e c \cos^2\Lambda (\Psi_1)^2 dx \quad (62)$$

$$\bar{k}_{\theta w} = -\int_0^L EB_2\gamma'\Psi_1'\Phi_1'' dx - q_\infty \int_0^L c_{L_\alpha} e c \tan\Lambda \cos^2\Lambda \Psi_1 \Phi_1' dx \quad (63)$$

$$\bar{k}_{w\theta} = -\int_0^L EB_2\gamma'\Phi_1''\Psi_1' dx + q_\infty \int_0^L c_{L_\alpha} c \cos^2\Lambda \Phi_1 \Psi_1 dx \quad (64)$$

$$\bar{k}_{ww} = \int_0^L EI_{yy}\left(\Phi_1''\right)^2 dx + q_\infty \int_0^L c_{L_\alpha} c \tan\Lambda \cos^2\Lambda \Phi_1 \Phi_1' dx \quad (65)$$

$$\bar{h}_{\theta\alpha} = q_\infty \int_0^L c_{L_\alpha} e c \cos\Lambda \Psi_1 dx \quad (66)$$

$$\bar{h}_{w\alpha} = -q_\infty \int_0^L c_{L_\alpha} c \cos\Lambda \Phi_1 dx \tag{67}$$

$$\bar{f}_\theta = -q_\infty \int_0^L c_{L_0} ec \cos^2\Lambda \Psi_1 dx + g \int_0^L \rho A e_{cg} \Psi_1 dx \tag{68}$$

$$\bar{f}_w = q_\infty \int_0^L c_{L_0} c \cos^2\Lambda \Phi_1 dx - g \int_0^L \rho A \Phi_1 dx \tag{69}$$

$$\bar{g}_{\theta,k} = -q_\infty \int_0^L \left(c_{m_{\delta_k}} c + c_{L_{\delta_k}} e \right) c \cos^2\Lambda \Psi_1 dx \tag{70}$$

$$\bar{g}_{w,k} = q_\infty \int_0^L c_{L_{\delta_k}} c \cos^2\Lambda \Phi_1 dx \tag{71}$$

Note that the bending-torsion divergence speed occurs when the stiffness matrix

$$\begin{bmatrix} \bar{k}_{\theta\theta} & \bar{k}_{\theta w} \\ \bar{k}_{w\theta} & \bar{k}_{ww} \end{bmatrix} = \begin{bmatrix} \bar{k}_{11} - q_\infty \Delta_{11} & \bar{k}_{12} - q_\infty \Delta_{12} \\ \bar{k}_{21} + q_\infty \Delta_{21} & \bar{k}_{22} + q_\infty \Delta_{22} \end{bmatrix} \tag{72}$$

is singular. Therefore the divergence speed is obtained from the solution of the following equation

$$\left(\Delta_{12}\Delta_{21} - \Delta_{11}\Delta_{22}\right) q_\infty^2 + \left(\bar{k}_{11}\Delta_{22} - \bar{k}_{22}\Delta_{11} + \bar{k}_{21}\Delta_{12} - \bar{k}_{12}\Delta_{21}\right) q_\infty + \left(\bar{k}_{11}\bar{k}_{22} - \bar{k}_{12}\bar{k}_{21}\right) = 0 \tag{73}$$

2. *Dynamic Analysis*

The weak-form integral expressions of the dynamic aeroelastic equations are obtained by multiplying the bending and torsion aeroelastic equations by $\Phi_i(x)$ and $\Psi_i(x)$, and then integrating over the wing span. This yields

$$\begin{aligned} &\sum_{j=1}^n \int_0^L \Psi_i \frac{d}{dx} \left\{ \left[GJ + EB_1 \left(\gamma'\right)^2 \right] \theta_j \Psi_j' - EB_2 \gamma' w_j \Phi_j'' \right\} dx = \\ &\sum_{j=1}^n \int_0^L \Psi_i \left[c_{L_\alpha} \left(\frac{\Delta\alpha}{\cos\Lambda} + \frac{q x_{ac}}{V_\infty \cos\Lambda} - w_j \Phi_j' \tan\Lambda - \theta_j \Psi_j - \frac{\dot{w}_j \Phi_j - e\dot{\theta}_j \Psi_j}{V_\infty \cos\Lambda} \right) + \sum_{k=1}^m \left(\frac{c}{e} c_{m_{\delta_k}} + c_{L_{\delta_k}} \right) \Delta\delta_k \right] e q_\infty \cos^2\Lambda c dx \\ &\qquad + \sum_{j=1}^n \int_0^L \Psi_i \rho I_{xx} \ddot{\theta}_j \Psi_j dx - \sum_{j=1}^n \int_0^L \Psi_i \rho A e_{cg} \ddot{w}_j \Phi_j dx \end{aligned} \tag{74}$$

$$\begin{aligned} &\sum_{j=1}^n \int_0^L \Phi_i \frac{d^2}{dx^2} \left(-EB_2 \gamma' \theta_j \Psi_j' + EI_{yy} w_j \Phi_j'' \right) dx = \\ &\quad \sum_{j=1}^n \int_0^L \Phi_i \left[c_{L_\alpha} \left(\frac{\Delta\alpha}{\cos\Lambda} + \frac{q x_{ac}}{V_\infty \cos\Lambda} - w_j \Phi_j' \tan\Lambda - \theta_j \Psi_j - \frac{\dot{w}_j \Phi_j - e\dot{\theta}_j \Psi_j}{V_\infty \cos\Lambda} \right) + \sum_{k=1}^m c_{L_{\delta_k}} \Delta\delta_k \right] q_\infty \cos^2\Lambda c dx \\ &\qquad - \sum_{j=1}^n \int_0^L \Phi_i \rho A \ddot{w}_j \Phi_j dx + \sum_{j=1}^n \int_0^L \Phi_i \rho A e_{cg} \ddot{\theta}_j \Psi_j dx \end{aligned} \tag{75}$$

Upon enforcing the zero boundary conditions at the two end points, the weak-form dynamic aeroelastic equations are obtained as

$$\begin{aligned} &\sum_{j=1}^n \int_0^L \Psi_i' \left\{ \left[GJ + EB_1 \left(\gamma'\right)^2 \right] \theta_j \Psi_j' - EB_2 \gamma' w_j \Phi_j'' \right\} dx \\ &+ \sum_{j=1}^n \int_0^L \Psi_i \left[c_{L_\alpha} \left(\frac{\Delta\alpha}{\cos\Lambda} + \frac{q x_{ac}}{V_\infty \cos\Lambda} - w_j \Phi_j' \tan\Lambda - \theta_j \Psi_j - \frac{\dot{w}_j \Phi_j - e\dot{\theta}_j \Psi_j}{V_\infty \cos\Lambda} \right) + \sum_{k=1}^m \left(\frac{c}{e} c_{m_{\delta_k}} + c_{L_{\delta_k}} \right) \Delta\delta_k \right] e q_\infty \cos^2\Lambda c dx \\ &\qquad + \sum_{j=1}^n \int_0^L \Psi_i \rho I_{xx} \ddot{\theta}_j \Psi_j dx - \sum_{j=1}^n \int_0^L \Psi_i \rho A e_{cg} \ddot{w}_j \Phi_j dx = 0 \end{aligned} \tag{76}$$

$$\sum_{j=1}^{n}\int_0^L \Phi_i''\left(-EB_2\gamma'\theta_j\Psi_j'+EI_{yy}w_j\Phi_j''\right)dx$$
$$-\sum_{j=1}^{n}\int_0^L \Phi_i\left[c_{L_\alpha}\left(\frac{\Delta\alpha}{\cos\Lambda}+\frac{qx_{ac}}{V_\infty\cos\Lambda}-w_j\Phi_j'\tan\Lambda-\theta_j\Psi_j-\frac{\dot{w}_j\Phi_j-e\dot{\theta}_j\Psi_j}{V_\infty\cos\Lambda}\right)+\sum_{k=1}^{m}c_{L_{\delta_k}}\Delta\delta_k\right]q_\infty\cos^2\Lambda c dx$$
$$+\sum_{j=1}^{n}\int_0^L \Phi_i\rho A\ddot{w}_j\Phi_j dx-\sum_{j=1}^{n}\int_0^L \Phi_i\rho Ae_{cg}\ddot{\theta}_j\Psi_j dx=0 \quad (77)$$

These equations can be expressed as

$$\sum_{j=1}^{n}\left(m_{\theta\theta,ij}\ddot{\theta}_j+m_{\theta w,ij}\ddot{w}_j+c_{\theta\theta,ij}\dot{\theta}_j+c_{\theta w,ij}\dot{w}_j+k_{\theta\theta,ij}\theta_j+k_{\theta w,ij}w_j+h_{\theta\alpha,i}\Delta\alpha+h_{\theta q,i}q\right)=\sum_{j=1}^{n}\sum_{k=1}^{m}g_{\theta,ik}\Delta\delta_k \quad (78)$$

$$\sum_{j=1}^{n}\left(m_{w\theta,ij}\ddot{\theta}_j+m_{ww,ij}\ddot{w}_j+c_{w\theta,ij}\dot{\theta}_j+c_{ww,ij}\dot{w}_j+k_{w\theta,ij}\theta_j+k_{ww,ij}w_j+h_{w\alpha,i}\Delta\alpha+h_{wq,i}q\right)=\sum_{j=1}^{n}\sum_{k=1}^{m}g_{w,ik}\Delta\delta_k \quad (79)$$

where

$$m_{\theta\theta,ij}=\int_0^L \rho I_{xx}\Psi_i\Psi_j dx \quad (80)$$

$$m_{\theta w,ij}=-\int_0^L \rho Ae_{cg}\Psi_i\Phi_j dx \quad (81)$$

$$m_{w\theta,ij}=-\int_0^L \rho Ae_{cg}\Phi_i\Psi_j dx \quad (82)$$

$$m_{ww,ij}=\int_0^L \rho A\Phi_i\Phi_j dx \quad (83)$$

$$c_{\theta\theta,ij}=\frac{1}{2}\rho_\infty V_\infty\int_0^L c_{L_\alpha}e^2c\cos\Lambda\Psi_i\Psi_j dx \quad (84)$$

$$c_{\theta w,ij}=-\frac{1}{2}\rho_\infty V_\infty\int_0^L c_{L_\alpha}ec\cos\Lambda\Psi_i\Phi_j dx \quad (85)$$

$$c_{w\theta,ij}=-\frac{1}{2}\rho_\infty V_\infty\int_0^L c_{L_\alpha}ec\cos\Lambda\Phi_i\Psi_j dx \quad (86)$$

$$c_{ww,ij}=\frac{1}{2}\rho_\infty V_\infty\int_0^L c_{L_\alpha}\cos\Lambda c\Phi_i\Phi_j dx \quad (87)$$

$$k_{\theta\theta,ij}=\int_0^L\left[GJ+EB_1\left(\gamma'\right)^2\right]\Psi_i'\Psi_j' dx-q_\infty\int_0^L c_{L_\alpha}ec\cos^2\Lambda\Psi_i\Psi_j dx \quad (88)$$

$$k_{\theta w,ij}=-\int_0^L EB_2\gamma'\Psi_i'\Phi_j'' dx-q_\infty\int_0^L c_{L_\alpha}ec\tan\Lambda\cos^2\Lambda\Psi_i\Phi_j' dx \quad (89)$$

$$k_{w\theta,ij}=-\int_0^L EB_2\gamma'\Phi_i''\Psi_j' dx+q_\infty\int_0^L c_{L_\alpha}c\cos^2\Lambda\Phi_i\Psi_j dx \quad (90)$$

$$k_{ww,ij}=\int_0^L EI_{yy}\Phi_i''\Phi_j'' dx+q_\infty\int_0^L c_{L_\alpha}c\tan\Lambda\cos^2\Lambda\Phi_i\Phi_j' dx \quad (91)$$

$$h_{\theta\alpha,i}=q_\infty\int_0^L c_{L_\alpha}ec\cos\Lambda\Psi_i dx \quad (92)$$

$$h_{\theta q,i}=\frac{1}{2}\rho_\infty V_\infty\int_0^L c_{L_\alpha}ecx_{ac}\cos\Lambda\Psi_i dx \quad (93)$$

$$h_{w\alpha,i}=-q_\infty\int_0^L c_{L_\alpha}c\cos\Lambda\Phi_i dx \quad (94)$$

$$h_{wq,i} = -\frac{1}{2}\rho_\infty V_\infty \int_0^L c_{L_\alpha} c x_{ac} \cos\Lambda \Phi_i dx \tag{95}$$

$$g_{\theta,ik} = -q_\infty \int_0^L \left(c_{m_{\delta_k}} c + c_{L_{\delta_k}} e \right) c \cos^2 \Lambda \Psi_i dx \tag{96}$$

$$g_{w,ik} = q_\infty \int_0^L c_{L_{\delta_k}} c \cos^2 \Lambda \Phi_i dx \tag{97}$$

The resultant matrix equation is obtained as

$$M\ddot{x}_e + C\dot{x}_e + Kx_e + Hx_a = G\Delta\delta \tag{98}$$

where $x_e = \begin{bmatrix} \theta_1 & \theta_2 & \cdots & \theta_n & w_1 & w_2 & \cdots & w_n \end{bmatrix}^\top$ is an elastic state vector of the generalized coordinates, $x_a = \begin{bmatrix} \Delta\alpha & q \end{bmatrix}^\top$ is an aerodynamic state vector of the angle of attack and pitch rate, $\Delta\delta = \begin{bmatrix} \Delta\delta_1 & \Delta\delta_2 & \cdots & \Delta\delta_n \end{bmatrix}^\top$ is a control vector of the incremental flap deflections, M is the generalized mass matrix, C is the generalized damping matrix, K is the generalized stiffness, H is the generalized aerodynamic coupling matrix, and G is the generalized force derivative vector due to the flap and slat deflections.

The generalized damping matrix is comprised of both the structural damping and the aerodynamic damping. The structural damping matrix can be obtained from a modal analysis that transforms the generalized coordinates into the modal coordinates via the eigenvalue analysis.

Consider the zero-speed structural dynamic equations

$$\ddot{x}_e + M^{-1}C_s\dot{x}_e + M^{-1}K_s x_e = M^{-1}F \tag{99}$$

where C_s is the structural damping matrix, K_s is the structural stiffness matrix corresponding to the stiffness matrix K at zero speed, and F is the force vector.

Assuming that the eigenvalues of the matrix $M^{-1}K_s$ are positive real and distinct, then by the similarity transformation, the matrix $M^{-1}K_s$ can be decomposed as

$$M^{-1}K_s = X\Omega^2 X^{-1} \tag{100}$$

where X is the eigenvector matrix and $\Omega = \mathrm{diag}\left(\omega_1, \omega_2, \ldots, \omega_n\right)$ is the diagonal matrix whose elements are the frequencies of the structural modes.

Let $q = X^{-1}x_e$ be the modal coordinates, then the transformed structural dynamics equation can be obtained as

$$\ddot{q} + X^{-1}M^{-1}C_s X\dot{q} + \Omega^2 q = X^{-1}F \tag{101}$$

which can be expressed in the modal coordinates as

$$\ddot{q}_i + 2\zeta_i\omega_i\dot{q}_i + \omega_i^2 q_i = f_i \tag{102}$$

where ζ_i is the damping ratio of the i-th mode.

Let $\zeta = \mathrm{diag}\left(\zeta_1, \zeta_2, \ldots, \zeta_n\right)$ be the damping ratio diagonal matrix, then the structural damping matrix is computed as

$$C_s = 2MX\zeta\Omega X^{-1} \tag{103}$$

The total damping matrix includes both the structural damping matrix and the aerodynamic damping matrix according to

$$C = C_s + C_a \tag{104}$$

where C_a is the aerodynamic damping matrix whose elements are defined by $c_{\theta\theta,ij}$, $c_{\theta w,ij}$, $c_{w\theta,ij}$, and $c_{ww,ij}$.

The aeroelastic modes of the aeroelastic equations are then obtained by the eigenvalue analysis of the following system:

$$\begin{bmatrix} \dot{x}_e \\ \ddot{x}_e \end{bmatrix} = \begin{bmatrix} 0 & I \\ -M^{-1}K & -M^{-1}C \end{bmatrix} \begin{bmatrix} x_e \\ \dot{x}_e \end{bmatrix} + \begin{bmatrix} 0 \\ M^{-1}\left(G\Delta\delta - Hx_a\right) \end{bmatrix} \tag{105}$$

The flutter boundary is defined to be an airspeed at which the real parts of the eigenvalues of the systems become zero.

IV. Coupled Aeroelastic Computation

To perform the coupled aeroelastic computation, the static aeroelastic model is coupled with Vorview through the automated vehicle geometry modeler. Aerodynamic force and moment coefficients as computed from Vorview are used as inputs to the static aeroelastic model. The computed aeroelastic deflections are then used to generate the aircraft deformed geometry by the automated vehicle geometry modeler. The aerodynamic solution is then recomputed with the aircraft deformed geometry in Vorview. This process is iterated until the solution is converged when errors in the computed aeroelastic deflections are within a specified tolerance. A flow chart for the coupled aeroelastic computation is shown in Fig. 9.

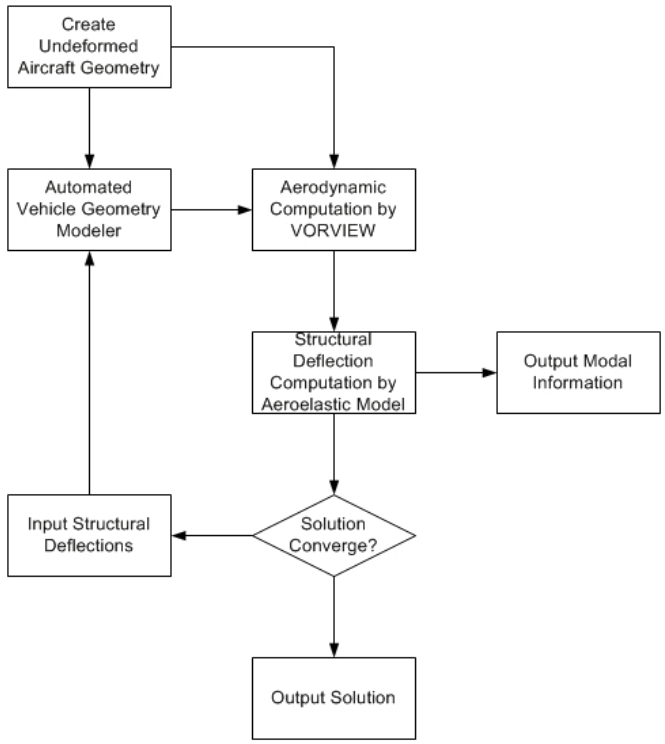

Fig. 9 - Coupled Aeroelastic Vortex Lattice Computation Flow Chart

The solution provides aerodynamic information for the deformed aircraft under static aerodynamic loading. The dynamic aeroelastic analysis can be used to estimate the unsteady contribution to wing aerodynamics. Given an atmospheric disturbance due to turbulence or a wind gust, or a time-varying motion of a flight control surface, the dynamic aeroelastic analysis can be used to compute the unsteady component of the aerodynamic force and moment coefficients.

Assuming steady state aerodynamics, the lift coefficient of an aircraft for symmetric flight can be expressed as

$$C_L(t) = C_{L_0} + \Delta C_{L_0} + C_{L_\alpha}\left[\bar{\alpha} + \Delta\alpha(t)\right] + C_{L_q} q(t) + C_{L_{\delta_k}} \delta_k(t) + \sum_{j=1}^{n} C_{L_{\theta_j}} \theta_j(t) + \sum_{j=1}^{n} C_{L_{w_j}} w_j(t) + \sum_{j=1}^{n} C_{L_{\dot{\theta}_j}} \dot{\theta}_j(t) + \sum_{j=1}^{n} C_{L_{\dot{w}_j}} \dot{w}_j(t) \quad (106)$$

where ΔC_{L_0} is the incremental lift coefficient at zero angle of attack due to static aeroelasticity obtained from the coupled solution, and $C_{L_{\theta_j}}$, $C_{L_{w_j}}$, $C_{L_{\dot{\theta}_j}}$, and $C_{L_{\dot{w}_j}}$ are the aeroelastic lift sensitivities

$$C_{L_{\theta_j}} = -\frac{2c_{L_\alpha}}{S}\int_0^L \cos^2\Lambda c \Psi_j dx \quad (107)$$

$$C_{L_{w_j}} = -\frac{2c_{L_\alpha}}{S}\int_0^L \tan\Lambda \cos^2\Lambda c \Phi_j' dx \quad (108)$$

$$C_{L_{\dot{\theta}_j}} = \frac{2c_{L_\alpha}}{V_\infty S}\int_0^L e\cos\Lambda c\Psi_j dx \tag{109}$$

$$C_{L_{\dot{w}_j}} = -\frac{2c_{L_\alpha}}{V_\infty S}\int_0^L \cos\Lambda c\Phi_j dx \tag{110}$$

The drag coefficient may be modeled by a parabolic drag polar

$$C_D(t) = C_{D_0} + \Delta C_{D_0} + \frac{C_L^2(t)}{\pi AR\varepsilon} \tag{111}$$

where ΔC_{D_0} is the incremental parasitic drag coefficient at zero lift due to static aeroelasticity obtained from the coupled solution, AR is the wing aspect ratio, and ε is the span efficiency factor.

For small drag contributions by the aeroelastic effects, the drag coefficient may be approximated as

$$\begin{aligned} C_D(t) &= C_{D_0} + \Delta C_{D_0} + \frac{\bar{C}_L^2}{\pi ARe} \\ &+ \frac{2\bar{C}_L}{\pi ARe}\left[C_{L_\alpha}\Delta\alpha(t) + C_{L_q}q(t) + C_{L_{\delta_k}}\delta_k(t) + \sum_{j=1}^n C_{L_{\theta_j}}\theta_j(t) + \sum_{j=1}^n C_{L_{w_j}}w_j(t) + \sum_{j=1}^n C_{L_{\dot{\theta}_j}}\dot{\theta}_j(t) + \sum_{j=1}^n C_{L_{\dot{w}_j}}\dot{w}_j(t)\right] \end{aligned} \tag{112}$$

where $\bar{C}_L$ is the trim lift coefficient

$$\bar{C}_L = C_{L_0} + \Delta C_{L_0} + C_{L_\alpha}\bar{\alpha} \tag{113}$$

In addition, the pitching moment coefficient of an aircraft is also influenced by the aeroelastic effects due to changes in wing lift characteristics. The pitching moment coefficient can be expressed as

$$\begin{aligned} C_m = C_{m_0} + \Delta C_{m_0} + C_{m_\alpha}[\bar{\alpha} + \Delta\alpha(t)] + C_{L_q}q(t) + C_{m_{\delta_k}}\delta_k(t) + \sum_{j=1}^n C_{m_{\theta_j}}\theta_j(t) + \sum_{j=1}^n C_{m_{w_j}}w_j(t) \\ + \sum_{j=1}^n C_{m_{\dot{\theta}_j}}\dot{\theta}_j(t) + \sum_{j=1}^n C_{m_{\dot{w}_j}}\dot{w}_j(t) \end{aligned} \tag{114}$$

where ΔC_{m_0} is the incremental pitching moment coefficient at zero angle of attack due to static aeroelasticity obtained from the coupled solution, and $C_{L_{\theta_j}}$, $C_{L_{w_j}}$, $C_{L_{\dot{\theta}_j}}$, and $C_{L_{\dot{w}_j}}$ are the aeroelastic lift sensitivities

$$C_{m_{\theta_j}} = \frac{2c_{L_\alpha}}{S\bar{c}}\int_0^L x_{ac}\cos^2\Lambda c\Psi_j dx \tag{115}$$

$$C_{m_{w_j}} = \frac{2c_{L_\alpha}}{S\bar{c}}\int_0^L x_{ac}\tan\Lambda\cos^2\Lambda c\Phi_j' dx \tag{116}$$

$$C_{m_{\dot{\theta}_j}} = -\frac{2c_{L_\alpha}}{V_\infty S\bar{c}}\int_0^L x_{ac}e\cos\Lambda c\Psi_j dx \tag{117}$$

$$C_{m_{\dot{w}_j}} = \frac{2c_{L_\alpha}}{V_\infty S\bar{c}}\int_0^L x_{ac}\cos\Lambda c\Phi_j dx \tag{118}$$

Thus, the aeroelastic deflections of the aircraft wings are coupled with aircraft dynamics through the angle of attack and pitch rate. The coupled system thus dictates both the aircraft responses as well as the aeroelastic deflections statically and dynamically.

V. Numerical Simulations

A Generic Transport Model (GTM) which represents a notional twin-engine, 200-passenger transport aircraft is used in the simulation study. The geometry is obtained by scaling up a 5.5% wind tunnel model of the GTM. Aerodynamic data for the sub-scale GTM are available from wind tunnel testing in NASA Langley's 14-ft by 22-ft wind tunnel.[9]

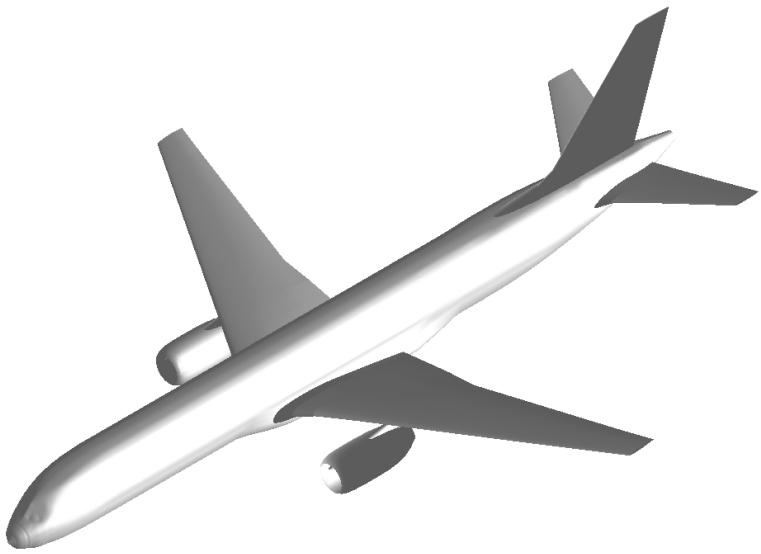

Figure 10 - Generic Transport Model

In general, structural information for commercial aircraft is not publicly available. Therefore, the uncertainty on the aeroelastic analysis can be high. Nonetheless, certain assumptions can be made for the structural stiffness of a wing if the wing deflection is known. In the study, the wing deflection for the GTM at 1-g loading at cruise is assumed to be about 3 ft at the tip. This is based on an extrapolation of the result of a structural certification test on a Boeing 777 wing. This wing deflected at the tip about 24 ft with an applied load of 3.75 g's. This corresponds to 1.5 times the design load which is established at 2.5 g's. The wing span of Boeing 777 is 200 ft and the wing span of the GTM is 124 ft. So the deflection of the Boeing 777 at 1-g loading is estimated to be about 6.4 ft by scaling the deflection by the loading ratio. The wing tip deflection for a cantilever beam with a different length L and structural stiffness EI is proportional to L^3/EI. Assuming that EI is proportional to $L^{3/2}$. Then, the wing tip deflection is proportional to $L^{3/2}$. Using this approximation, the GTM wing is modeled as equivalent beam structure with a mass density that results in the correct wing weight. The Young's modulus and shear modulus are then adjusted by trial and error until the desired wing tip deflection is obtained. The distributions of the GTM wing structural stiffness values are plotted in Figures 11 and 12.

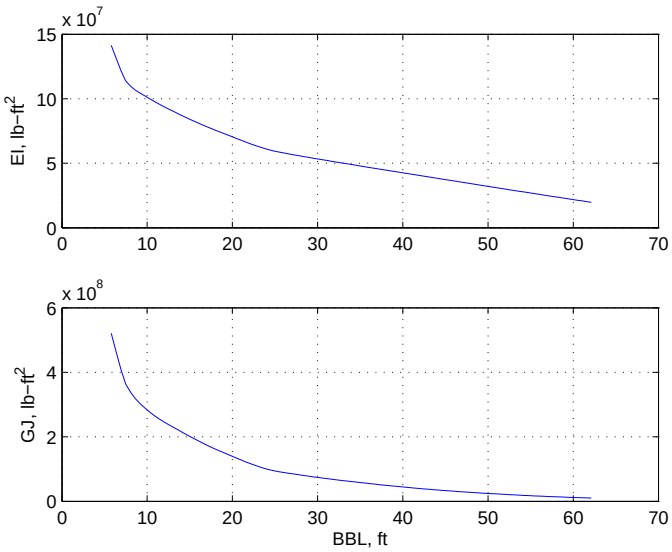

Figure 11 - Estimated Wing Bending and Torsional Stiffness

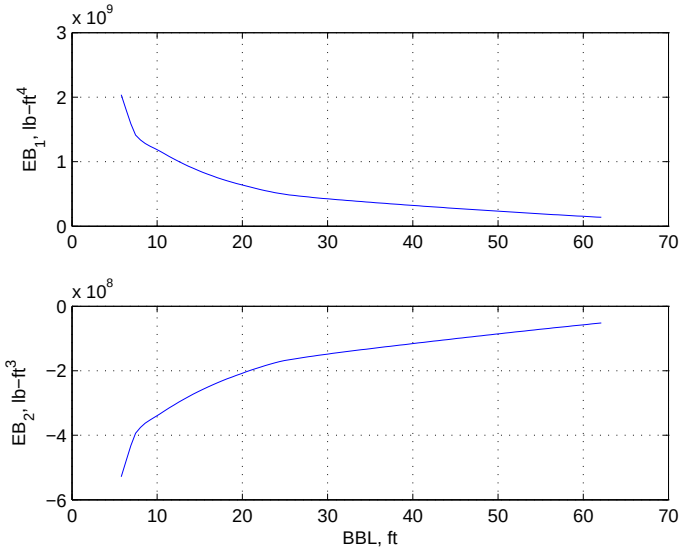

Figure 12 - Estimated Wing Bending-Torsion Coupling Stiffness

A. Static Aeroelastic Response

The aircraft weighs 175,000 lbs and cruises at mach 0.8 at 30,000 ft. The initial trim angle of attack with no aeroelastic deflection is 2.05°. After 4 iterations, the trim angle of attack is 0.80° as shown in Table 1. Thus, the aeroelastic deflections effectively contributes 1.25° to the angle of attack of the aircraft. The wing tip bending and torsional deflections are 3.064 ft vertically upward and 2.204° nose up as shown in Figure 13. Figures 14 and 15 are the plots of the pressure coefficient C_p distributions for the rigid aircraft and the flexible aircraft. Because of the effective increase in the attack of attack, the pressure loading on the wing also increases for the same angle of attack of the aircraft. It is also noticed that the drag coefficient increases when the aeroelastic effects are present. The increase in drag is probably due to changes in the induced drag associated with changes in the wing lift distribution caused by the aeroelastic deflections.

Iteration	α, deg	C_{L_0}	C_{L_α}	C_L	C_D	C_{m_α}	C_m	$\bar{W}_{tip}$, ft	$\bar{\Theta}_{tip}$, deg
1	2.0498	0.0899	6.3931	0.3186	0.0090	-1.7619	-0.1852	3.0592	-2.2049
2	0.7984	0.2297	6.3755	0.3186	0.0155	-1.7227	-0.1540	3.0641	-2.2041
3	0.8039	0.2288	6.3970	0.3186	0.0155	-1.7150	-0.1540	3.0582	-2.2051
4	0.7982	0.2298	6.3756	0.3186	0.0155	-1.7227	-0.1539	3.0640	-2.2041

Table 1 - Coupled Aeroelastic-Vorview Solution

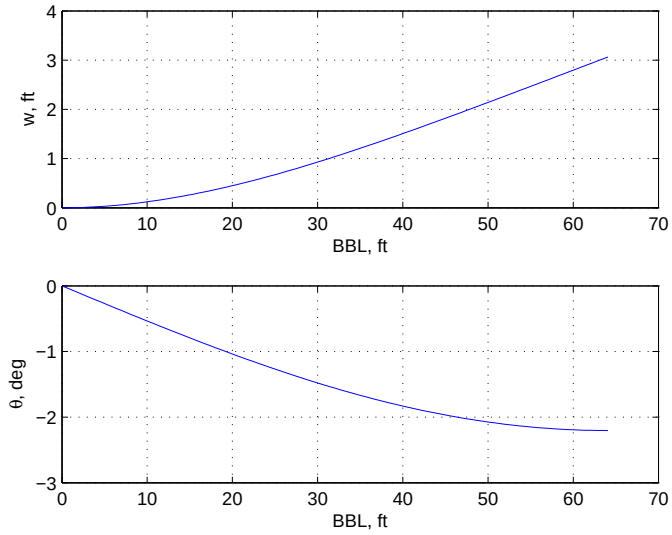

Figure 13 - Wing Aeroelastic Deflections

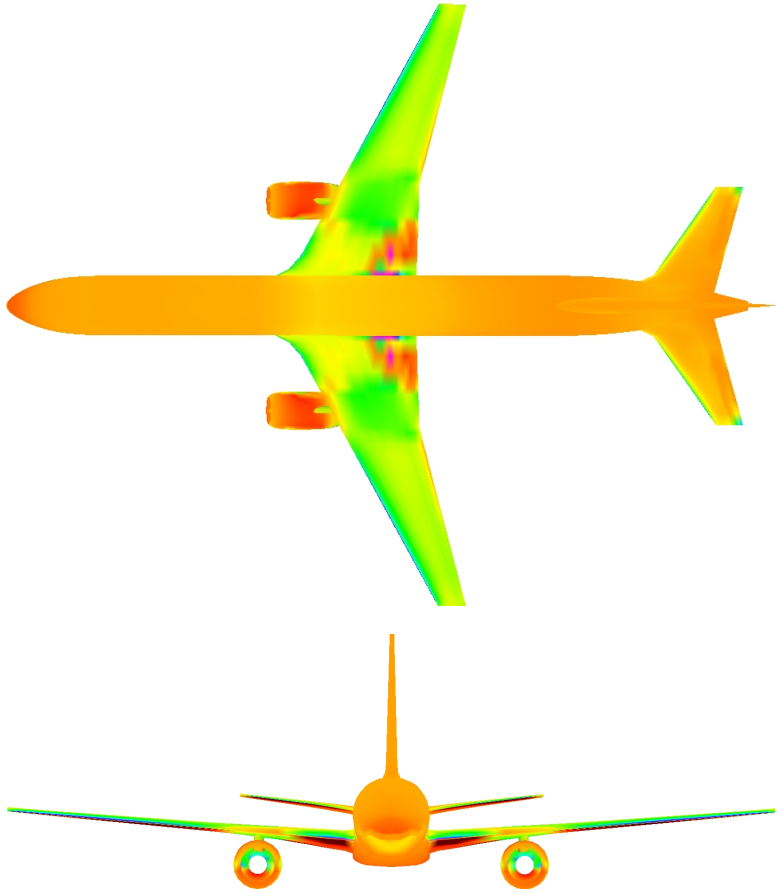

Figure 14 - C_p Distribution for Rigid Aircraft

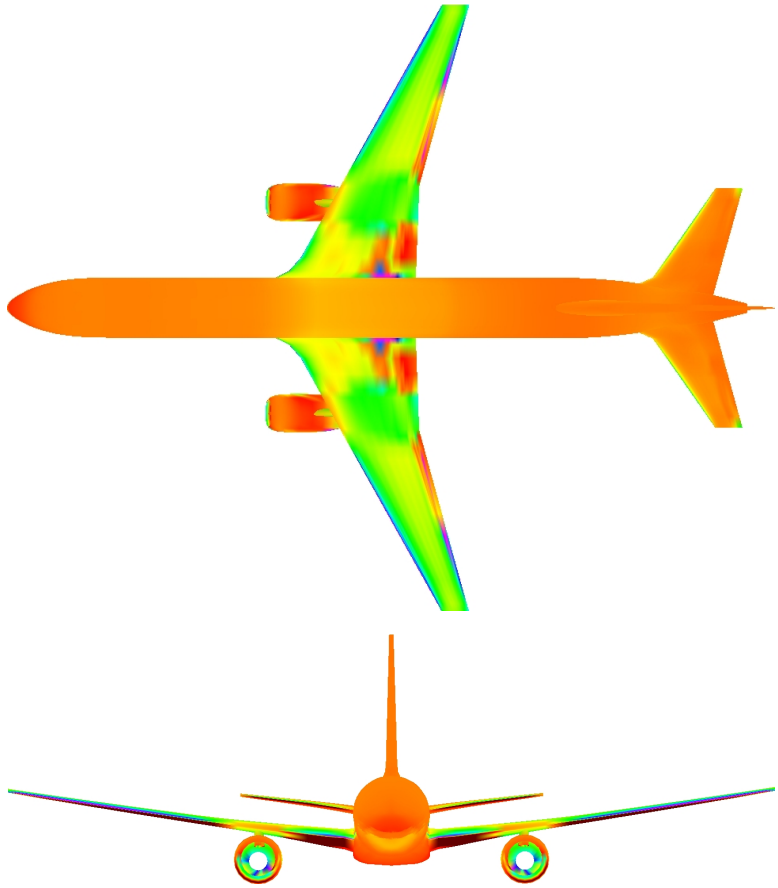

Figure 15 - C_p Distribution for Flexible Aircraft

B. Dynamic Aeroelastic Response

The dynamic motion of the wing is assumed to be predominantly due to the first bending and torsion modes. The forcing function is assumed to be a light vertical wind gust with a turbulence intensity based on the Dryden turbulence model.[10] The vertical wind speed w_a and the turbulent pitch rate q_a are shown in Figures 16 and 17.

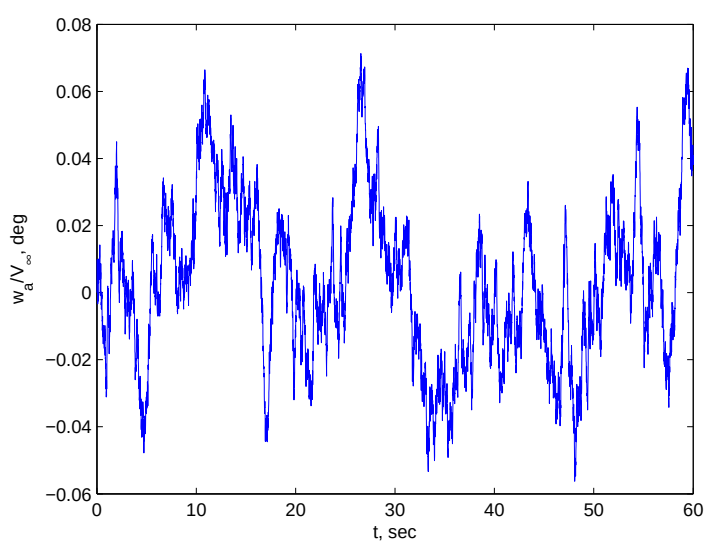

Figure 16 - Turbulence Vertical Wind Speed

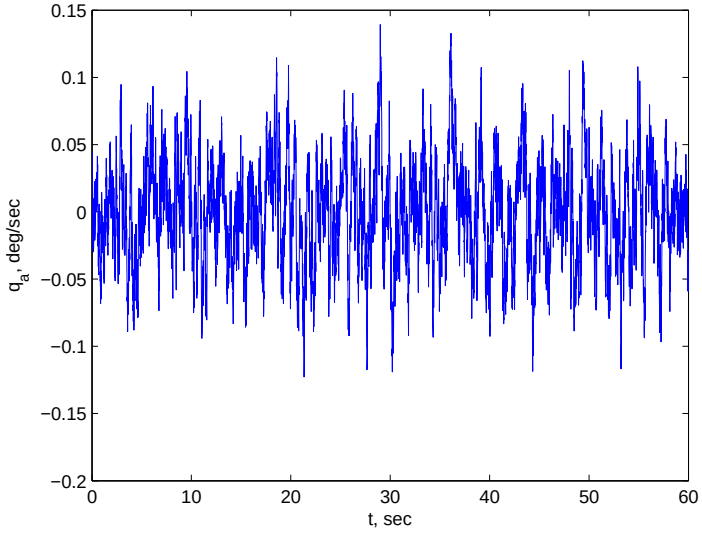

Figure 17 - Turbulence Pitch Rate

The time varying angle of attack and pitch rate act as sources of excitation to the aircraft wings. The structural damping is assumed to be $\xi = 0.2$. This structural damping corresponds to a flutter speed at Mach 0.845. The first symmetric bending mode is at 9.0 rad/sec with a damping of 0.16, while the first symmetric torsion mode is at 11.8 rad/sec with a damping of 0.37. The aircraft incremental angle of attack, pitch rate, and wing tip dynamic bending and torsional deflections are plotted in Figures 18 through 21. The aircraft unsteady lift coefficient, drag coefficient, and pitching moment coefficient are plotted in Figures 22, 23, and 24.

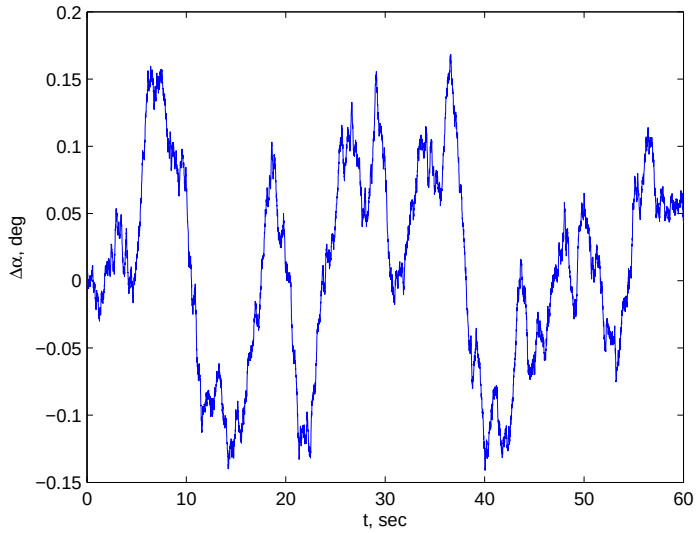

Figure 18 - Angle of Attack

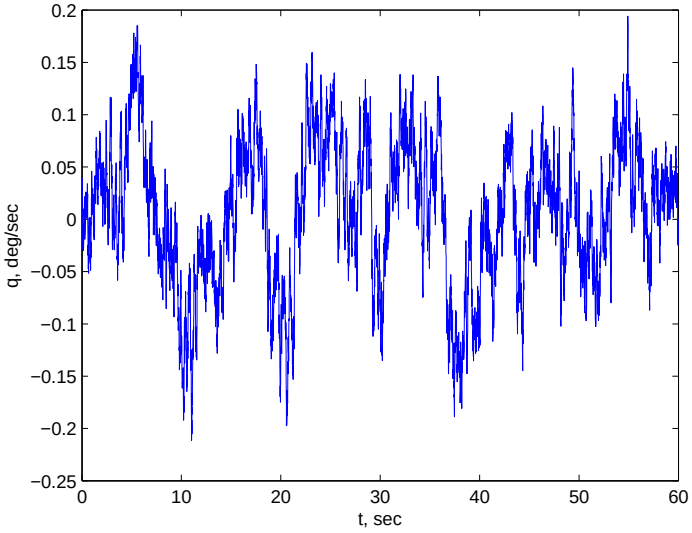

Figure 19 - Pitch Rate

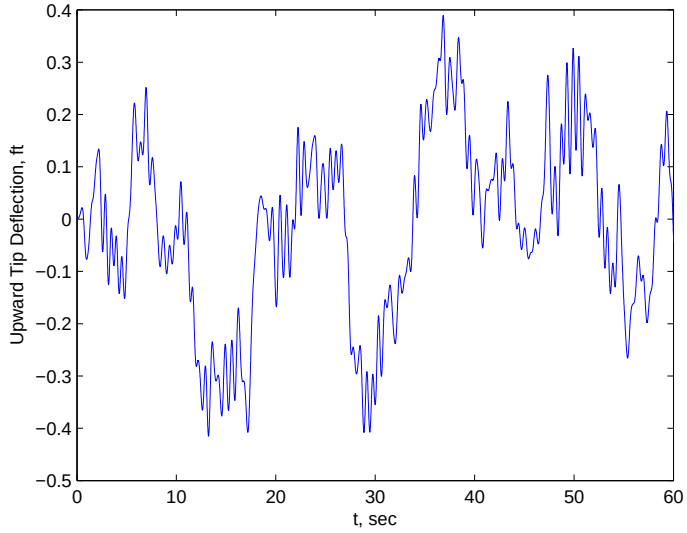

Figure 20 - Wing Bending Deflection

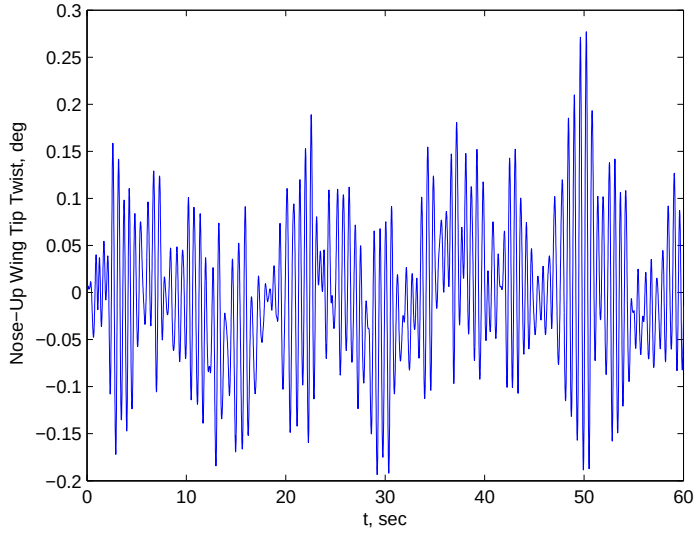

Figure 21 - Wing Torsional Deflection

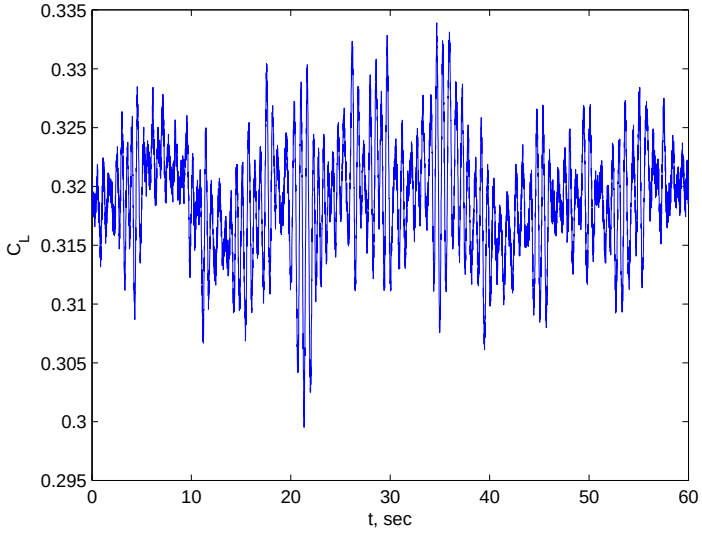

Figure 22 - Aircraft Unsteady Lift

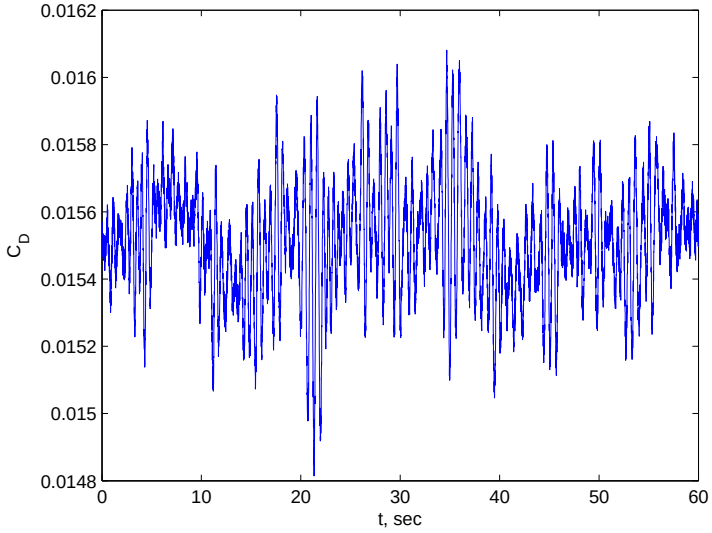

Figure 23 - Aircraft Unsteady Lift Coefficient

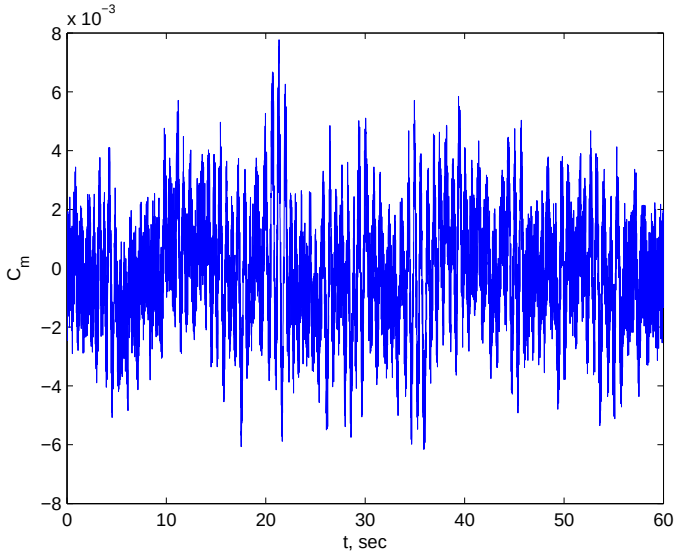

Figure 24 - Aircraft Unsteady Pitching Moment Coefficient

VI. Discussion

The coupling between the vortex-lattice code and the aeroelastic model is facilitated by an external geometry modeler. While this approach is reasonable, perhaps an alternative implementation is to actually incorporate an aeroelastic model directly into a vortex-lattice formulation. The advantage of the alternative approach is that the static aeroelastic effects on aerodynamic characteristics are probably more accurately predicted as the aeroelastic contribution to the angle of attack is properly accounted for. Moreover, using a dynamic aeroelastic response model, a quasi-unsteady aerodynamic model of an aircraft could be constructed to properly estimate the unsteady downwash effect of the wings on the tail plane. In the present approach, this downwash effect is not accounted for, so the dynamic aeroelastic response solution only provides the wing-alone contribution to the overall aerodynamic characteristics of the aircraft. The disadvantage of the alternative approach is the complex numerical implementation that requires a truly coupled numerical solution at the algorithmic level that integrates an aeroelastic solution method with the vortex-lattice method.

Future work will extend the present method using the unsteady aerodynamic methods of Theodorsen and or Peters for the aeroelastic analysis. Furthermore, the asymmetric aeroelastic motion would be developed in the future work.

VII. Conclusion

This paper presents a coupled aeroelastic and vortex-lattice aerodynamic modeling approach for analyzing aerodynamic and aeroelastic characteristics of flexible aircraft. The vortex-lattice code Vorview provides a rapid aerodynamic prediction tool for preliminary aircraft concept studies. With the addition of static and dynamic aeroelastic capability, the prediction tool is further capable of analyzing aerodynamics of flexible aircraft configurations. The aeroelastic model estimates the effects of the coupled wing bending-torsion motion on the aircraft aerodynamics. The aeroelastic angle of attack is a function of the elastic deflections of the wing in bending and torsion. This causes airspeed dependent frequencies and damping that give rise to wing divergence and flutter. A generic transport model is used to demonstrate the tool capability. The coupled aeroelastic and vortex-lattice solution provides the static aeroelastic deflections of the wings which result in changes in the aircraft trim angle of attack, and lift and drag characteristics. A dynamic aeroelastic model with a turbulent wind gust is computed separately to estimate quasi-unsteady aerodynamics of the aircraft.

References

[1]Miranda, L.R., Elliot, R.D., and Baker, W.M., "A Generalized Vortex Lattice Method for Subsonic and Supersonic Flow Applications," NASA CR-2865, 1977.

[2]Nguyen, N. T., Nelson, A., and Pulliam, T., "Damage Adaptive Control System Research Report," Internal NASA Report, April 2006.

[3]Aftosmis, M. J., Berger, M. J., and Melton, J. E., "Robust and Efficient Cartesian Mesh Generation for Component- Based Geometry," AIAA Journal, Vol. 36, No. 6, 1998, pp. 953-960.

[4]Hodges, D.H. and Pierce, G.A., *Introduction to Structural Dynamics and Aeroelasticity*, Cambridge University Press, 2002.

[5]Nguyen, N. T., "Integrated Flight Dynamic Modeling of Flexible Aircraft with Inertial Force-Propulsion-Aeroelastic Coupling," AIAA-2008-194, 46th AIAA Aerospace Sciences Meeting, Reno, NV, Jan 2008.

[6]Houbolt, J. C. and Brooks, G. W., "Differential Equations of Motion for Combined Flapwise Bending, Chordwise Bending, and Torsion of Twisted Nonuniform Rotor Blades," NACA Technical Note 3905, February 1957.

[7]Theodorsen, T. and Garrick, I.E., "Mechanism of Flutter - a Theoretical and Experimental Investigation of the Flutter Problem", NACA Report 685, 1940.

[8]Tuzcu, I., Nguyen, N., "Aeroelastic Modeling and Adaptive Control of Generic Transport Model," AIAA Atmospheric Flight Mechanics, AIAA-2010-7503, August 2010.

[9]Jordan, T. L., Langford, W. M., Belcastro, C. M., Foster, J. M., Shah, G. H., Howland, G., and Kidd, R., "Development of a Dynamically Scaled Generic Transport Model Testbed for Flight Research Experiments," AUVSI Unmanned Unlimited, Arlington, VA, 2004.

[10]Schmidt, L. V., *Introduction to Aircraft Flight Dynamics*, AIAA Education Series, 1998.